4.3.1 Cathode at Reference Temperature

The polarization of the cathode at reference temperature $T^{\diamond} = 298\,\mathrm{K}$ is shown on fig. 4.4. It is obvious that it is not possible to came close to the measured data with a pure *Butler-Volmer* based model (first curve "No Flooding - No LM-Region"). The resulting polarization curves are necessarily concave due to the mathematical nature of the e-function in use (the *Butler-Volmer equation*). But being aware that there is a well known flooding problem on the cathode, cf. [45, 108], the introduction of a flooding model as described in 2.4.3 on page 35 makes sense (second curve "Flooding - No LM-Region"). In the next step it is taken into account, that there is a sharp change of the kinetic at the transition from the *Temkin* to the *Langmuir adsorption region* at the transition potential $\mathscr{U}_{tr}$ near 0.8 V vs. RHE (third curve "Flooding - with LM-Region", cf. chap. 2.4.1). With the flooding model and the *Langmuir adsorption region* there are three additional fit parameters:
Begin of flooding j_{fl}, flooding fraction Θ_{fl} and the *transfer coefficient* in the Langmuir adsorption region $\alpha_{\mathrm{OR},LM}$. The fit at $T^{\diamond}$ was done in two stages, first ξ_{eo}, $\check{I}^{\diamond 0}$, α_{OR}, j_{fl}, Θ_{fl} in the *Temkin region* and in the second stage $\alpha_{\mathrm{OR},LM}$ in the *Langmuir region*. The decline of α from the *Temkin* to the *Langmuir* potential domain is expected, but it is with 10% smaller than the expected 45±5% [88]. The value of the fitted $\alpha_{lm} = 0.66$ at 333 K corresponds to data in literature, it is only 5 % under the value published by PARTHASARATHY [88][1].

4.3.2 Electrode and Cell Polarization at Varied Temperatures

The OCP of the cathode in fig. 4.6 is decreasing with temperature because of increasing methanol diffusion through the membrane, due to the rise of the temperature dependent diffusion transport of methanol across the membrane. But this trend changes at higher current densities. Fig. 4.5 demonstrates, that the methanol oxidation on the anode raises with temperature and increasing polarization. This causes a decline of methanol concentration at the membrane surface, hence, the crossover flow thins down. The diamond symbol $\diamond$ in fig. 4.6 lies on the crossing point of the 298 and 333 K curves.

The polarization curves of the full cell in fig. 4.7 show the expected increase of the current density at a given fuel cell voltage with rising temperature. But the increase of current density slows down with growing temperature, this is caused by the opposite trend of the cathode polarization, as is visible in fig. 4.6.

Fig. 4.5: Anode potential vs. RHE at varied temperatures. The transfer coefficient is temperature dependent $\alpha = \alpha^{\diamond} \cdot (T - T^{\diamond})$, it decreases from 0.56(T = 298 K) down to 0.38 (T = 353 K)

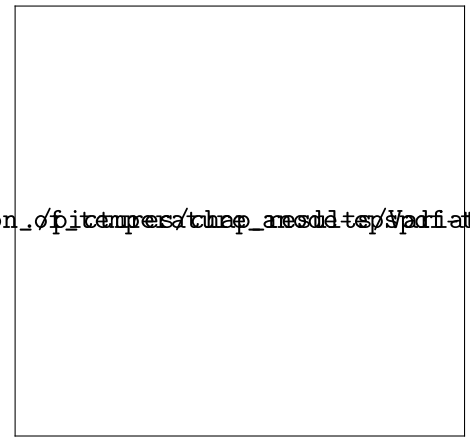

Fig. 4.6: Cathode potential vs. RHE at varied temperatures. It is interesting that the polarization curves for 298 and 333 K cross at current density of $j = 448.0$ A/m^2, the crossing is marked with a diamond $\diamond$.

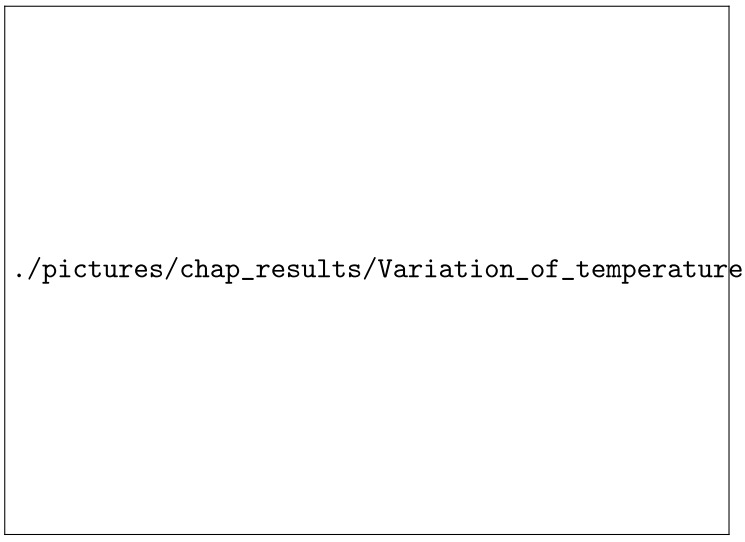

Fig. 4.7: Fuel cell polarization at varied temperature.

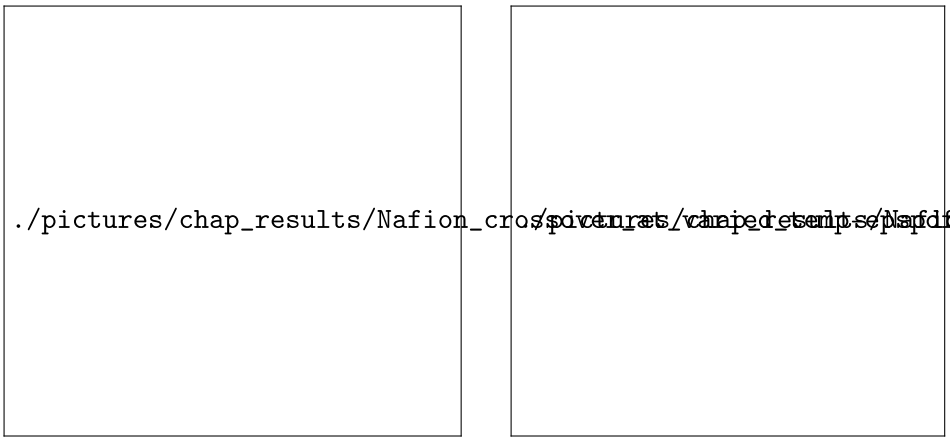

Fig. 4.9: Current density equivalents of methanol crossover (on the left) and carbon dioxide drag from anode to cathode side (on the right).
Membrane type: Nafion™117, stoichiometry factors: λ_{AN}(@1000 A/m^2)= 1.7, λ_{CA}(@1000 A/m^2)= 5.8.

4.4 Crossover at Varied Temperature

Beside the methanol crossover, there is also a carbon dioxide crossover from the anode across the membrane. The transport mechanisms for both are comparable: they are the electroosmotic drag and the diffusion. Both transport modes depend mainly on the species concentration at the anodic membrane surface. In the model assumptions we define the state of aggregation for water at the membrane surface as liquid, thus the concentration is limited by the species solubility in water or in the water-methanol mixture. The solubility of methanol in water is ideal, but the solubility of carbon dioxide is declining with temperature. Despite the superimposition of these two flows one method to determine the methanol crossover, is the measurement of carbon dioxide in the cathode off-gas. This method is described by VALDEZ and NARAYANAN[119]. As mentioned in chap. 2.3.3 DOHLE [35] reported, that the CO_2-crossover at low methanol feed concentrations ($c_{CH_3OH} \leq 1$ M) and high current densities ($j_{fc} > 2000$ A/m^2) can exceed the methanol crossover. Hence, the model differentiate between three carbon dioxide flows in the cathode off-gas: a) atmospheric, b) CO_2-drag and c) product gas from the cathodic methanol oxidation. In fig. 4.9 the flows b) and c) are depicted for steady anode and cathode supply. The results are qualitative comparable to the measurements of VALDEZ and NARAYANAN[119] and the simulation of WANG and WANG [127]. The simulation results for the CO_2-drag (right graph fig. 4.9) furthers the practice to gauge the methanol crossover behavior of a DMFC by measuring the CO_2-off-gas concentration: the CO_2-drag is below 5 % of the product gas from the cathodic

[1] α_{lm} = 0.66 ≙ -0.112 V/decade Δj_{OR}, cf. eq. 2.22 on page 32